NANO LETTERS

2006
Vol. 6, No. 8
1674−1681

Influence of Polymer-Blend Morphology on Charge Transport and Photocurrent Generation in Donor–Acceptor Polymer Blends

Jarvist M. Frost, Fabien Cheynis,† Sachetan M. Tuladhar, and Jenny Nelson*

Department of Physics, Imperial College London, The Blackett Laboratory, Prince Consort Road, London SW7 2BW, U.K.

Received April 13, 2006; Revised Manuscript Received June 6, 2006

ABSTRACT

Monte Carlo algorithms are used to simulate the morphologies adopted by polymer chains in a polymer-blend film in the limits where the chains are mutually attractive (homophilic regime) and mutually repulsive (heterophilic regime) and then to simulate the drift transport of charges through the polymer chains. In the homophilic regime, chains aggregate into tangled domains resulting in a relatively high percolation threshold, a high density of configurational trap states, and slow, dispersive charge transport. In the heterophilic regime at the same polymer volume fraction, chains self-organize into a lacework pattern resulting in a low percolation threshold and efficient, trap-free charge transport. For homophilic morphologies interchain hopping is rate-limiting and mobility is insensitive to chain length, whereas for heterophilic morphologies intrachain transport is important and mobility increases with increasing chain length. The morphologies are used in simulations of photocurrent quantum efficiency for donor–acceptor blend photodiodes, which show that the effects of morphology on charge pair generation and recombination compete with the effect on transport, such that the optimum blend composition is sensitive to both morphology and recombination rate. We conclude that it is essential to consider the connectivity of and morphology adopted by polymer chains in the optimization of materials for organic solar cells.

Binary blends of conjugated molecular materials are of growing interest for applications to light-emitting and photovoltaic devices. Donor−acceptor blends consisting of two conjugated polymers,[1] a polymer and a conjugated molecule,[2] or a polymer and inorganic nanocrystals[3] have been demonstrated to achieve effective photocurrent generation, and blends of two polymers can be used to achieve efficient light emission.[4] For application to solar cells or photodetectors, the large interface between the two components acts to dissociate excitons that have been photogenerated in either material, thereby generating separate charges that can travel to different electrodes and so deliver a photocurrent. For application to polymer light-emitting devices, the two components are responsible for transporting electrically injected charges toward the interface, where charge association and radiative recombination may occur. The morphology of the blend formed by the two components is thus critical to device function in each case. In this paper, we present the first study of the influence of polymer-blend morphology on the drift transport and photocurrent generation efficiency in a blend of polymer chains with a second material.

For both solar cells and LEDs, the requirement of high and balanced electron and hole mobilities in the blend material is of critical importance to device performance. However, the few existing studies of charge transport in organic donor−acceptor blends indicate that transport in the blend material is not easily predicted from the transport properties of the component materials in isolation,[5,6] with the result that the dependence of device performance on blend composition is difficult to predict.[7] Among the factors that may influence charge transport in polymer−molecule or polymer−polymer blends are the different morphologies adopted by the two components, particularly in the case where one is a high molecular weight polymer and the other is a "small" conjugated molecule. However, there is no theoretical apparatus with which to model charge transport in such asymmetric-blend materials. The widely used Gaussian disorder model (GDM) due to Baessler[8] and its variants[9,10] are successful at describing the gross features of drift transport in disordered systems in terms of a number of disorder-related parameters, but these parameters have a physical meaning only for a cubic lattice of hopping sites. Configurational disorder is present as a distribution of

* Corresponding author. Tel: +44 20 7594 7581. Fax: +44 20 7581 3817. E-mail: jenny.nelson@imperial.ac.uk.

† Now at: Laboratoire Louis Néel, CNRS, BP166, F-38042 Grenoble Cedex 9, France.

10.1021/nl0608386 CCC: $33.50
Published on Web 07/07/2006

temperature-independent hopping rate coefficients, but bears no clear relation to the physical or chemical structure of the materials used. Two-phase organic systems have been modeled as a binary blend of monomers arranged on a cubic lattice, where the lattice is generated either as a random binary blend[11−13] or through a Metropolis Monte Carlo simulation of the equilibrium thermodynamics of the interface.[14,15] The latter method allows the physics of the interfacial interactions between like and unlike components to be incorporated through the specific interaction energies, and, by varying these energies relative to each other and to the thermal energy, kT, allows binary morphologies that are mixed, segregated, or random to be generated. Such models have been useful for demonstrating the influence of compositional heterogeneity on drift transport[11] and on photocurrent quantum efficiency[15] and the influence of annealing[14] and interfacial interaction energies[15] on morphology. However, all of these studies treat each organic material as a collection of independent monomers on a cubic lattice; none of these approaches are capable of treating polymer chains.

The fact that polymers exist as connected chains of monomers influences both the type of morphology that can be achieved and the nature of charge transport. With regard to morphology, chain connectedness and chain entanglement limit the degree of mixing or segregation that can be achieved for given specific interaction energies. With regard to transport, the extension of localized electronic states along the polymer backbone may lead to different hopping rates, on average, for charge hops along rather than between polymer chains. Both of these effects can be modeled if we represent the polymer chains as jointed chains of monomers on a cubic lattice. Previous studies[16] have shown that the tendency of chains to segregate or mix, and other statistical mechanical properties, can be modeled using Monte Carlo (MC) simulations of the equilibrium configuration of mobile, interacting jointed chains on a cubic lattice.

We consider a model system consisting of a number of polymer chains or "snakes" embedded in a "sea" of unconnected units (monomers) of another material. The snakes are self-avoiding, jointed chains of L cubic units and are mounted on a cubic lattice. All remaining lattice sites are assigned to sea. The total interaction energy, E_{total}, is given by the sum of nearest-neighbor interaction energies, ΣE_{ij}, where E_{ij} takes different values for intermolecular snake−snake (E_{aa}) and snake−sea (E_{ab}) interfaces, and the sea−sea interaction is set to zero. Because the snakes remain of constant length through the simulations, the permanent intramolecular snake−snake contribution is constant and can be ignored. Snakes are capable of "slithering" by moving either head or tail by one step at random into any of the available nearest-neighbor positions and allowing the rest of the snake to follow. Effectively, this means chopping off the monomer in the tail position and replacing it in the position to which the head is to move, or vice versa. Snakes can freely displace the sea, but each lattice site can be occupied by only one snake monomer. The morphology simulation proceeds via a Metropolis MC algorithm as follows. Initially, a number of snakes of length L that corresponds to the intended volume density, ρ, is inserted into the simulation volume in random configurations and E_{total} is computed. The initial, random configuration represents the state of the system in equilibrium at high temperature, T, irrespective of the interaction energies. For each snake move, a snake is selected at random, a forward move of either the head or the tail of the snake is selected at random, and the change in total interaction energy, ΔE, that would result from that move is calculated. Note that ΔE consists only of the changes in interaction energy that result from moving the old tail into the new head position; interactions due to the rest of the snake are not changed. The move is performed, and E_{total} is updated, if $\gamma < \exp(-\Delta E/kT)$ where γ is a random number between 0 and 1 and k is Boltzmann's constant. This moving procedure is repeated many times for values of T, E_{aa}, and E_{ab}. We focus on the contrasting cases of mutually repulsive snakes (the heterophilic regime) where $E_{\text{aa}} > E_{\text{ab}}$, and mutually attractive snakes (the homophilic regime) where $E_{\text{aa}} < E_{\text{ab}}$, with small thermal fluctuations (such that $\Delta E \geq kT$) in each case. Progress toward equilibrium morphology is monitored by means of an aggregation factor χ, defined as the average fraction of nearest-neighbor interactions that are like−like. The simulation is stopped after typically 10^9 snake moves and the coordinates of the snakes are stored. Simulations for larger numbers of snake moves led to no further changes in χ for the heterophilic morphology and an extremely slow increase in segregation for the homophilic case. This procedure produced contrasting morphologies for the two regimes, as discussed below.

Time-of-flight (ToF) photocurrent transients are simulated by the method described in ref 17, which makes use of a continuous time random walk (CTRW) to handle multiple charge carriers and allow for charge trapping. We consider only the case of hole transport within the snake material, to represent, for example, hole transport in a donor-type polymer in a blend. A number (typically 200) of charge carriers is generated uniformly on snake sites over the 100 lattice planes closest to the blocking electrode to simulate charge generation by a laser pulse. Hole hopping is allowed only between snake monomers with a transition rate of

$$\Gamma_{ij} = \nu_0 \exp(-(\Delta G - e\mathbf{F}\cdot\mathbf{r}_{ij} - \lambda)^2/4\lambda kT) \exp(-2r_{ij}/r_0) \quad (1)$$

where ν_0 takes the value ν_{inter} (ν_{intra}) for inter- (intra-) chain hops, λ represents the reorganization energy, $\mathbf{F}$ is the applied electric field vector, $\mathbf{r}_{ij}$ is the unit vector joining initial and final sites, and r_0 is the localization radius estimated from calculations of the dependence of the electronic transfer integral on separation between conjugated oligomers.[18] ΔG takes the value 0 in all cases because disorder in site energies is not considered. The waiting time, τ_n, for the nth charge is calculated as

$$\tau_n = -\ln \gamma/\Sigma_i \Gamma_{in} \quad (2)$$

where γ is a random number between 0 and 1 and the sum is taken over all neighboring sites i of snake type within a

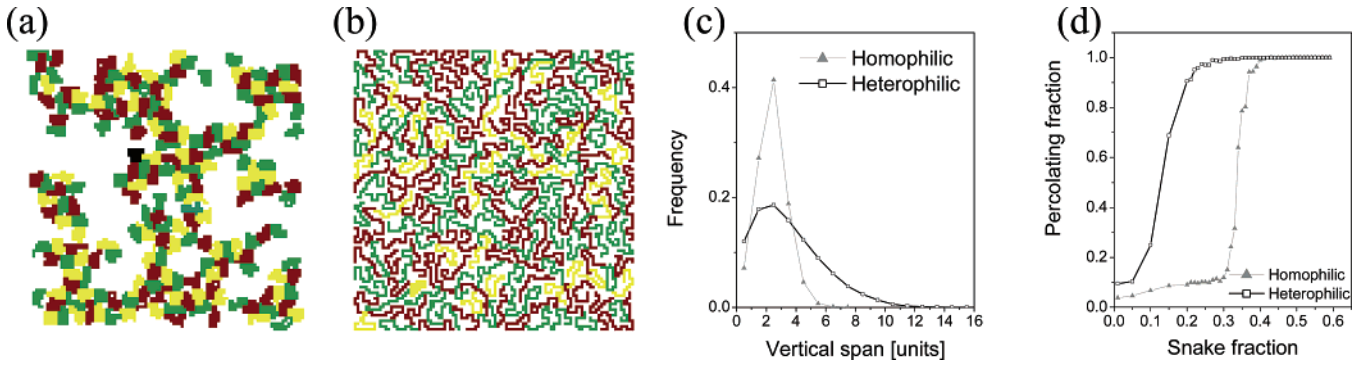

Figure 1. (a and b) Typical morphologies generated in two-dimensional (100 × 100 units) space in the limits of (a) homophilic snakes ($E_{aa} = -kT$, $E_{ab} = 0$) and (b) heterophilic snakes ($E_{aa} = kT$, $E_{ab} = 0$). The snakes are all 25 units long, and the volume fraction of snake is $\rho = 0.50$ in each case. (c) Frequency plot of the vertical (z direction) span by snakes of length 25 on a three-dimensional (50 × 50 × 1000 units) lattice, for homophilic ($E_{aa} = -kT$, $E_{ab} = 0$) (triangles) and heterophilic ($E_{aa} = kT$, $E_{ab} = 0$) (squares) morphologies. (d) Fraction of snake sites that belong to a percolating cluster (i.e., in contact with one electrode) for homophilic (triangles) and heterophilic (squares) lattices.

sphere of radius $r \leq 2$ units. The destination is chosen in proportion to the probability

$$P_i = \Gamma_{in}/\Sigma_i \Gamma_{in} \tag{3}$$

If the destination is occupied by a charge carrier, then another destination is chosen. If all destinations are occupied, then the hopper sleeps in its current location for the time τ_n. Charges are sorted into order of waiting times and moved according to a CTRW algorithm.[19] Moves in the positive or negative field direction are registered and added or subtracted from the induced photocurrent. The simulation is repeated around 10 times for the same parameters and an average current transient is built up. The transit time, t_{tr} , is determined as the intersection time of two linear asymptotes drawn to the current−time plot on a double logarithmic representation, according to the customary definition for analysis of experimental data.[20] Mobility is defined as $\mu = d^2/t_{tr} F$ where d is the film thickness. ToF simulations are carried out on lattices of dimensions 50 × 50 × 1000 units, with non-periodic boundary conditions in the x and y directions, a blocking boundary at $z = 0$, and a collecting boundary at $z = 1000$. The lattice unit a is taken to represent 1 nm, in accordance with typical polymer densities. ν_0 is taken as 10^{13} s^{-1}, r_0 as 0.3 nm, and λ as 0.5 eV, in accordance with quantum chemical calculations[18] and previous simulations.[17] The electric field is applied in the positive z direction.

For photocurrent quantum efficiency, a lattice with a thickness of 50 units is used to represent a thin (50 nm) film. Electron transport is permitted in the sea material and hole transport in the snakes. Excitons are generated continuously at a volume generation rate G. To focus on the effects of morphology, exciton generation is spatially uniform and equal absorption coefficients are used for unoccupied sea and unoccupied snake sites. Excitons dissociate if a free site of the opposite material is found within a distance L_{ex} of the generation site, where L_{ex} represents the exciton diffusion length. Upon dissociation, the exciton is replaced by an electron (hole), if the exciton was generated in sea (snake) material, and the free snake (sea) site is occupied with the opposite type charge, that is, hole (electron). If no free site is found for dissociation, then the exciton is removed immediately, representing geminate recombination by excitons that fail to diffuse to an interface. Electrons (holes) diffuse by performing a random walk between available sea (snake) sites within a radius of 2 units, with a total hopping probability of $p_{hop} = 6D\Delta t/a^2$ in a time step of length Δt where D is the charge diffusion coefficient. The destination site is chosen at random in proportion to $\exp(-2r_{ij}/r_0)$ where r_{ij} is the separation of initial and final sites and r_0 is defined above. Multiple site occupation is forbidden. When a charge steps into a site adjacent to a charge of opposite type, recombination occurs with a probability of $k_{rec}\Delta t$ per time step and both charges are removed from the lattice. Electrons that reach the electron collecting ($z = 0$) interface and holes that reach the hole collecting ($z = 50$) interface are collected and contribute to the photocurrent. The simulation is started with some arbitrary electron and hole population and run until steady state is reached. An average steady-state photocurrent is then found from the time-average of the steady-state electron or hole current, averaged over several simulations, using different realizations of the lattice.

The contrast between the homophilic and heterophilic regimes is illustrated by typical morphologies obtained on two-dimensional lattices and shown in Figure 1. For the homophilic case $E_{aa} = -kT$ and $E_{ab} = 0$, whereas for the heterophilic case $E_{aa} = kT$ and $E_{ab} = 0$. The two-dimensional plots illustrate the essential contrast between the two cases: attractive snake interactions lead to aggregation of snakes into large domains, whereas repulsive snake interactions lead to dispersion of snakes into isolated strands in the sea, which develop into a lacework pattern at snake densities close to the percolation threshold. The same behavior is seen in three dimensions.[21] In the homophilic morphology, snakes tend to coil up, whereas in the heterophilic morphology they tend to adopt a looser, uncoiled, and self-avoiding form. This is quantified in Figure 1c by frequency plots of the span along the z axis of snakes of length 25 units in homophilic compared with heterophilic lattices. For the homophilic morphology, the span peaks at the average diameter of the

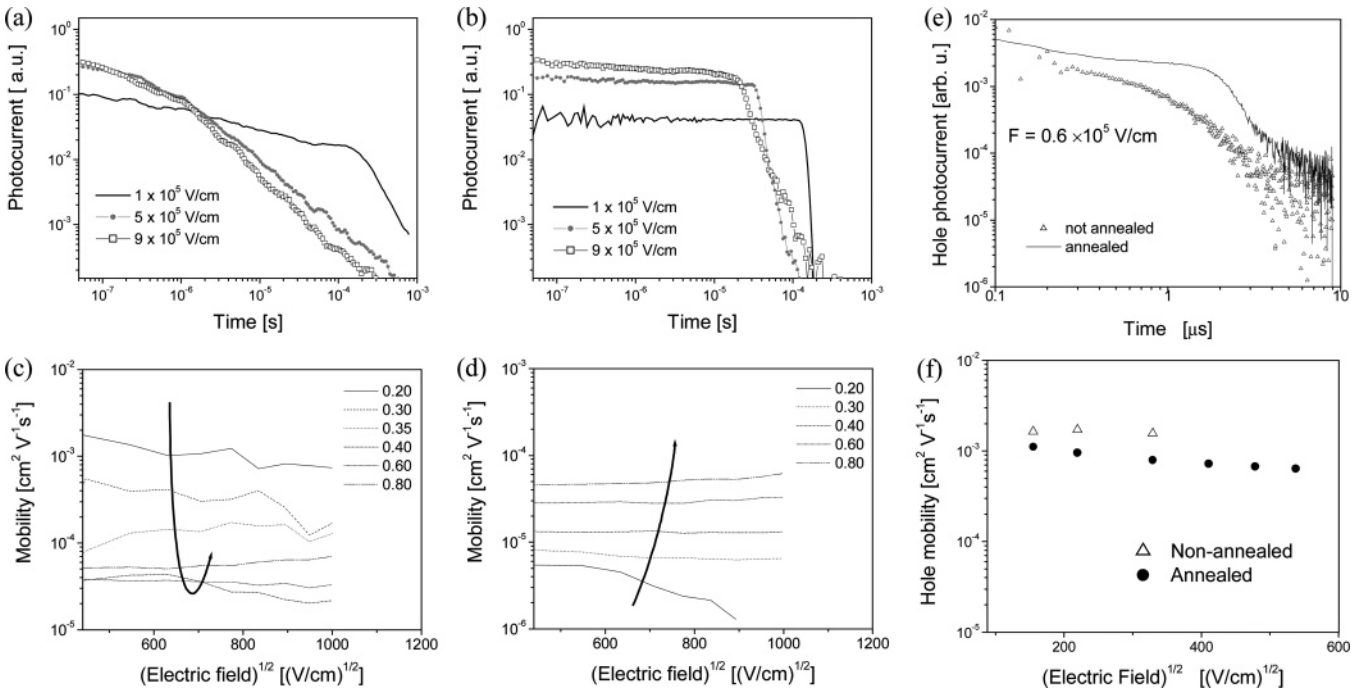

Figure 2. (a and b) Simulated time-of-flight (hole) photocurrent transients at three different applied electric fields, for (a) homophilic and (b) heterophilic morphologies with snake density of $\rho = 0.3$. (c and d) Poole−Frenkel plots of mobility as a function of square root of electric field, for (c) homophilic and (d) heterophilic lattices of varying snake density. The arrows indicate the trend with increasing snake density. The snake length is 25 units in all cases. Inter- and intrasnake hopping rates are equal. (e) Measured hole photocurrent transient for a thin (830 nm) film of poly(9,9′ dioctylfluorene) before (triangles) and after (full line) annealing at 125 ° C (above the glass transition temperature of the polymer). Details of sample preparation and measurement are the same as those in ref 23. The change in shape is consistent with the polymer chains adopting a less tangled morphology upon annealing. (f) Poole−Frenkel plots of the hole mobility for the sample in e, before (triangles) and after (circles) annealing.

ball formed when the snake coils up, whereas for the heterophilic morphology, much longer spans are likely. The longer reach of snakes in the heterophilic morphology leads to a lower threshold for percolation. Figure 1d shows that the threshold for nearest-neighbor site percolation occurs at a snake density ρ of only 0.1−0.2 for the heterophilic morphology, compared to 0.33 for the homophilic morphology, and 0.31 for nearest-neighbor site percolation on an infinite 3D cubic lattice. We will show below that the uncoiled nature of the snakes in the heterophilic morphology can lead to more efficient charge transport.

Different morphologies lead to different time-of-flight photocurrent transients. Figure 2a and b shows ToF transients for homophilic and heterophilic morphologies, respectively, both made with $\rho = 0.30$ and $L = 25$ nm and with equal inter- and intrasnake hopping rates ($\nu_{inter} = \nu_{intra} = \nu_0$). In both cases, traces for different electric fields show that transport becomes faster with increasing electric field, as expected. For the heterophilic morphology, the transient shows a plateau with an abrupt decay after a certain time, characteristic of nondispersive transport where photogenerated charges move together with similar velocity, to reach the collecting electrode after a well-defined transit time. For the homophilic morphology, transport shows a monotonic decay with a change in slope, shown by a "knee" on the double logarithmic plot. Such transients are characteristic of dispersive transport where a wide range of site-to-site hopping times leads to a wide range of effective carrier velocities and of arrival times at the collecting electrode. The different behaviors can be explained by noting that, for any given snake density, there are fewer different transport paths through a homophilic than a heterophilic morphology (i.e., poorer percolation), and therefore a higher probability that charges will become trapped at bottlenecks or dead ends in the homophilic morphology, leading to a wider range of arrival times. This was confirmed by studying the distribution of paths taken by charges during transport, discussed below. The dispersive behavior is pronounced for the density used in Figure 2a ($\rho = 0.3$) because it is close to the percolation threshold for homophilic lattices. At higher snake densities, the transients on homophilic lattices for a given electric field become less dispersive, until in the limit of large ρ ($\rho >$ 0.8) transients for both homophilic and heterophilic lattices become identical and sheet-like. This is a clear demonstration of how configurational disorder can lead to dispersive transport.

An additional consequence of configurational disorder is the slow tail that develops in the heterophilic lattice transients at high electric fields. This is due to the trapping to charges in dead ends in the lattice, where the charges must hop against the applied field to escape, and the rate of escape reduces as electric field is increased. Similar behavior is seen for homophilic lattices at higher ρ where the transport is less dispersive. Transients that become more dispersive with increasing electric field have been observed in some heterogeneous experimental systems. This is a consequence of the heterogeneous nature of the lattice and underlines the need for a two-phase model.

Figure 2c and d also illustrates the consequences of determining the mobility from dispersive transients. For all cases, t_{tr} is determined as the intercept of the long-time and short-time linear asymptotes to the current transient on a double logarithmic plot. Although the transport on the homophilic lattice is clearly more dispersive than that on the heterophilic lattice of the same density, the apparent mobility, derived from this definition of t_{tr} , is higher by 1 to 2 orders of magnitude at low densities. As ρ increases, the mobility obtained for nondispersive, sheetlike transport on the heterophilic morphologies increases, as would be expected from the increasing effective cross-sectional area for charge transport. Yet over the same range, the apparent mobility obtained from the dispersive transients on the homophilic morphologies *decreases* until the density ($\rho \approx 0.5$) at which transport becomes nondispersive, and then increases. This comparison shows how the value of mobility obtained using the above definition of t_{tr} can be misleading and illustrates the dangers of comparing mobility values for dispersive and nondispersive materials. Similar phenomena have been seen in experiment, where mobility appears to decrease upon treating the material in a way that improves order and makes transport less dispersive. An example is shown in Figure 2e and f for a thin film of a high hole mobility conjugated polymer, poly(9,9′-dioctylfluorene) before and after annealing above its glass transition temperature. Detailed studies of this material have confirmed that this annealing treatment promotes crystallinity and increases the hole mobility in thick (>1 μm) films.[23] However, thin (<1 μm) films tend to show dispersive transport before annealing with fast transit times and high apparent mobilities. The effect of annealing on such films is to *increase* t_{tr} and *reduce* the apparent mobility value. From the comparison of these data with the simulation results in Figure 2a and b, we propose that the transport behavior in thin films before annealing results from a more tangled chain morphology similar to the homophilic regime, whereas that observed after crystallization and in thicker films results from more extended, uncoiled chain morphology. The decrease in apparent mobility with increasing electric field that has been reported for several experimental systems[24] may similarly be partly due to the definition of t_{tr}.

The very different transient shapes for ToF photocurrent transients on homophilic and heterophilic morphologies indicate that there is a much wider dispersion in the hopping times for charges on a homophilic than a heterophilic lattice and suggest that on a homophilic lattice there are fewer available low resistance paths between the electrodes. This was investigated by monitoring the time-averaged occupation probability of each snake monomer on a lattice of 50 × 50 × 50 units during a time-of-flight simulation for homophilic and heterophilic lattices each of $\rho = 0.3$. Trajectory maps, generated by inputing the data as a density map into PovRAY,[25] are presented in Figure 3. These show that in the heterophilic morphology most parts of the snake lattice were visited with uniform probability. In the homophilic morphology, contrast is visible between inaccessible sea domains (dark) and regions of high occupation probability

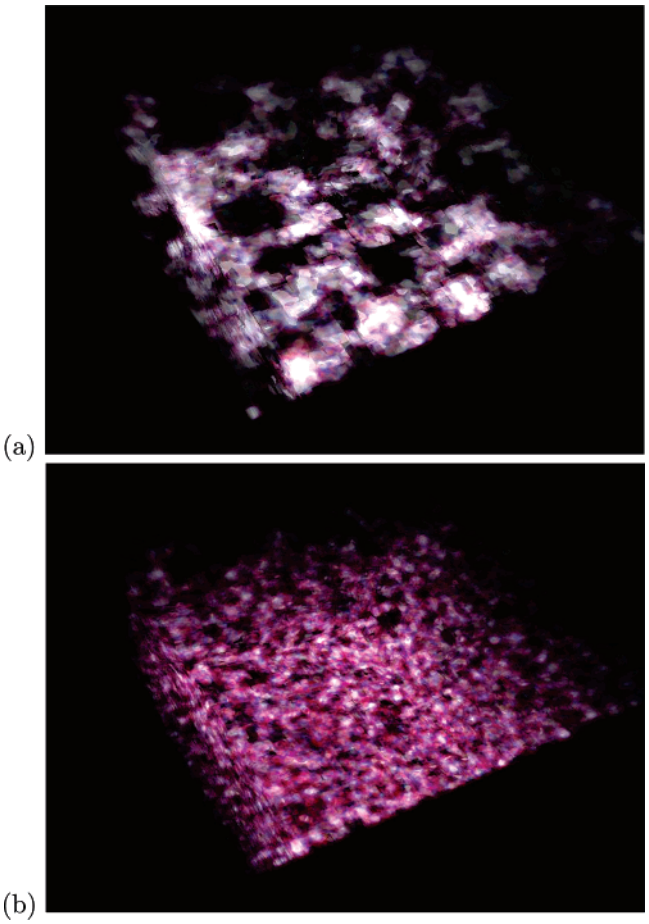

Figure 3. Time-averaged occupation probabilities for snake sites during a time-of-flight simulation with 400 charges at $F = 1 \times 10^5$ V cm^{-1} on (a) a homophilic lattice and (b) a heterophilic lattice, each of density $\rho = 0.3$. Brighter regions represent higher occupation probabilities and indicate charge traps. In each figure, the charges are injected in the first five planes on the left-hand side of the cube and collected at an electrode on the right-hand side. Generated from density map using PoVRAY.[25]

(bright) that act as charge traps in the snake material, with only a few efficient transport paths of low occupation probability.

An interesting question is then the contribution of intrasnake as opposed to intersnake hops. In conjugated polymers, it is reasonable to expect that the electronic transfer integrals for charge transfer between neighboring conjugated segments on the same polymer backbone will be larger than those for transfer between conjugated segments on different polymer chains. Therefore, we investigate the effect of making the coefficient for hops within the same snake faster, by a factor of 100, than that for hops between different snakes, that is, $\nu_{intra} = \nu_0 = 100\nu_{inter}$. Figure 4 a and b shows the effect of this on transients for homophilic and heterophilic lattices ($\rho = 0.3$). Figure 4a shows that this change accelerates transients on homophilic lattices only slightly, and only at low fields when the transient is relatively nondispersive. For dispersive transients, the effect is negligible. This indicates that the rate-limiting steps in these dispersive transients are intersnake hops. For the heterophilic lattice, where transport is nondispersive, Figure 4b shows that the transient is

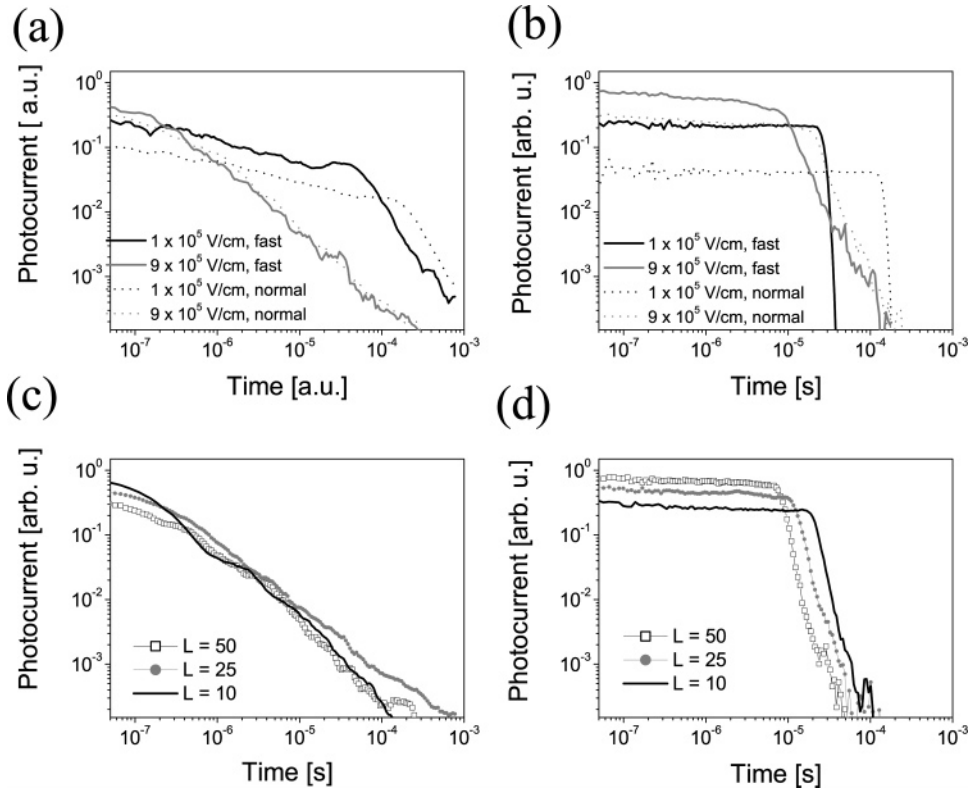

Figure 4. (a and b) Simulated time-of-flight photocurrent transients for an intrasnake hopping rate that is equal to ("normal") and 100 times faster than ("fast") the intersnake hopping rate, at two different applied electric fields, for (a) homophilic and (b) heterophilic morphologies with snake densities of $\rho = 0.3$. The snake length is 25 units in both cases. (c and d) Simulated time-of-flight photocurrent transients for fast hopping ($\nu_{intra} = 100*\nu_{inter}$) on snake lattices of different snake length and $\rho = 0.3$ for (c) homophilic and (d) heterophilic morphologies. The electric field is 5×10^5 V/cm in both cases.

accelerated by up to an order of magnitude at low field. Intrachain hops therefore contribute much more significantly to the transport on heterophilic than homophilic lattices. This is in good agreement with the average snake span data presented in Figure 1d: charges can travel, on average, further along a single snake in a heterophilic than in a homophilic lattice. For practical applications, this suggests that in materials where interchain charge transfer is relatively slow, transport can be optimized by blending the polymer into a medium that encourages separation of the chains.

The above results also indicate that, in materials where intrachain exceeds interchain hopping, transport should benefit from increased snake length mainly in heterophilic morphologies. Figure 4c and d shows the effects of snake length on transients for homophilic and heterophilic lattices ($\rho = 0.3$), where $\nu_{intra} = \nu_0 = 100\nu_{inter}$. For heterophilic lattices, increasing the chain length from $L = 10$ nm to $L = 50$ nm more than doubles the mobility (Figure 4d), whereas for homophilic lattices, chain length has no significant effect. Indeed, longer chains tend to degrade the transport, possibly as a result of more compacted morphology. The result is relevant to experimental studies of the effect of polymer molecular weight (MW) on charge mobility. FET mobilities of poly-3-hexylthiophene thin films of different molecular weight showed that mobility tends to increase with MW but that the MW also influences morphology (e.g., crystallinity) of the polymer, which has a secondary influence on mobility.[26,27] The present work confirms that morphology must be considered when assessing the effect of varying MW on charge transport in polymers.

The superior transport in heterophilic compared to homophilic morphologies suggests that higher short-circuit currents may be available from donor−acceptor blend photodiodes with heterophilic morphology. However, the morphology also influences both charge separation efficiency and charge recombination rates through its influence on the interfacial area. To investigate the net effect of morphology on a photovoltaic device, we simulate the photocurrent generation under steady-state illumination for model devices based on homophilic and heterophilic morphologies of different density. The morphologies could represent donor−acceptor blends where the donor is a conjugated polymer, represented here by the snakes, and the acceptor is an isotropic small molecule, represented here by the sea. We use a short ($L_{ex} = 1$ nm) exciton diffusion length to exaggerate the effects of morphology on charge-pair generation. Exciton generation is uniform, and both materials absorb light with equal probability. Therefore, any asymmetry in the composition dependence of photocurrent generation must be due to the effects of morphology. We use an incident photon flux density of 1.25×10^{17} cm^{-2} s^{-1}, an absorption coefficient of 10^5 cm^{-1}, and a diffusion coefficient of $D = 8.3 \times 10^{-9}$ cm^2 s^{-1} (corresponding to a zero field mobility of around 3×10^{-7} cm^2 V^{-1} s^{-1}, typical of polyphenylenevinylene polymers[5]) for each material in the bulk. Figure 5 compares the resulting photocurrent internal quantum ef-

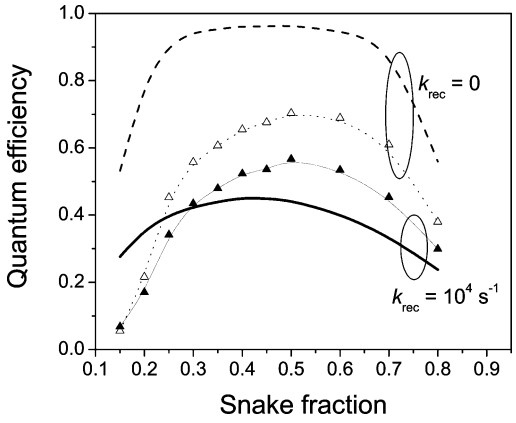

Figure 5. Simulated photocurrent internal quantum efficiency as a function of snake density, for homophilic (triangles) and heterophilic (lines) lattices, (a) without recombination (homophilic: open triangle, heterophilic: dashed line) and (b) with a nearest-neighbor recombination rate of 10^4 s^{-1} (homophilic, filled triangle; heterophilic, full line). Simulations are carried out on a 50-nm-thick film with perfectly selective electrodes, with a photogeneration rate of 1.25×10^{17} $cm^{-2}s^{-2}$, an exciton diffusion length of 1 nm, and zero-field charge mobilities of 3×10^{-7} cm^2 V^{-1} s^{-1}. The snake length is 25 units in all cases. Inter- and intrasnake hopping rates are equal.

ficiency (*IQE*) using homophilic and heterophilic morphologies, as a function of ρ, for the cases of no electron−hole recombination and the case of a nearest-neighbor recombination rate of $k_{rec} = 10^4$ s^{-1}, which is well within the range of recombination rates observed in experimental bulk heterojunction blends.[28,29] *IQE* is defined here as the ratio of the steady-state electron flux passing through the electrodes to the product of the incident photon flux and the film absorbance.

In the case of no recombination, *IQE* is controlled only by the exciton dissociation efficiency and is not influenced by charge transport. Figure 5 shows that with no recombination the heterophilic morphology leads to higher photocurrent generation over all blend compositions. The heterophilic morphology presents a larger internal interfacial area than the homophilic, and the probability of finding an interface within 1 nm of exciton generation is close to unity over a wide range of ρ, whereas in the homophilic morphology, snake aggregation into domains larger than L_{ex} means that excitons generated in the interior of snake domains are unlikely to dissociate. The fall off of *IQE* at high and low ρ for both morphology types is due to inefficient charge pair generation for the low interface areas at those densities. Morphological differences due only to different domain size are exaggerated at low ($\rho < 0.5$) snake densities, whereas as ρ approaches 1 the morphologies tend to the same limit.

In the case of typical nearest-neighbor recombination rate ($k_{rec} = 10^4$ s^{-1}), the *IQE* is suppressed by recombination in each case but to a much higher degree for heterophilic than homophilic morphologies. Now the maximum *IQE* is determined by competition between transport and recombination. In the heterophilic morphology, charge transport is faster (despite the lower *apparent* mobilities) but recombination is also faster, on account of the higher interfacial area. Figure 5 shows that for this value of k_{rec} the advantage of faster transport in the heterophilic morphology is outweighed by the disadvantage of faster recombination for densities $\rho > 0.3$. This observation is in accord with recent experimental results on poly-3-hexylthiophene−PCBM blends where the recombination rate is found to be very much lower than that expected for a Langevin process if the two materials in the blends were in intimate contact.[30] The explanation proposed there, of domain formation inhibiting recombination, is quite compatible with the simulation results presented here. There is clearly an optimization problem in the design of morphologies for efficient photocurrent generation, as previous simulation studies have also shown.[13,15] Although some of the previous studies of charge dynamics in polymer−fullerene blends[28,29] have concluded that transport and recombination are controlled by the same processes in those cases, this relationship can be altered by asymmetric blend morphologies.

In summary, we have studied the influence of polymer-blend morphology on charge transport and photocurrent generation in polymer blends using Monte Carlo simulation methods. By varying the interaction energies between the chains, contrasting morphologies consisting of well dispersed, loosely coiled polymer chains (heterophilic) or aggregated, tightly coiled chains (homophilic) can be produced, representative of morphologies of polymer films following different types of process treatment (solvent, annealing). The morphology strongly influences charge transport characteristics, such that homophilic blends show a lower threshold for charge percolation and more dispersive transport than heterophilic blends, consistent with a higher probability of charge trapping in configurational traps. Experimental observations, such as the effect of annealing on charge transients in some conjugated polymers, can be explained by our model in terms of process-induced changes in polymer morphology, whereas monomer-based transport models cannot explain the data. We have also shown that the mobility extracted from the position of the knee on a double logarithmic plot of a ToF transient may be an overestimate in the case of dispersive transport, stressing the need for more detailed models to interpret the behavior of disordered experimental systems. In simulations of photocurrent generation in polymer-blend solar cells, we find that morphology influences both transport and charge recombination such that the optimum composition and morphology is a sensitive function of charge recombination and separation rates. Faster transport, achieved through optimizing the blend morphology, does not necessarily lead to higher photocurrent generation. More refined versions of these MC models, developed for specific experimental systems, could be extremely valuable for the optimization of materials for polymer-blend devices.

Acknowledgment. We are grateful to James Kirkpatrick, Jonny Williams, and Amanda Chatten for useful discussions.

References

(1) Halls, J. J. M.; Walsh, C. A.; Greenham, N. C.; Marseglia, E. A.; Friend, R. H.; Moratti, S. C.; Holmes, A. B. *Nature* **1995**, *376*, 498−500.
(2) Brabec, C. J.; Sariciftci, N. S.; Hummelen, J. C. *Adv. Funct. Mater.* **2001**, *11*, 15−26.

(3) Milliron, D. J.; Gur, I.; Alivisatos, A. P. *MRS Bull*. **2005**, *30*, 41−44.
(4) Moons, E. *J. Phys.: Condens. Matter* **2002**, *14*, 12235−12260.
(5) Tuladhar, S. M.; Poplavskyy, D.; Choulis, S. A.; Durrant, J. R.; Bradley, D. D. C.; Nelson, J. *Adv. Funct. Mater*. **2005**, *15*, 1171−1182.
(6) Mihailetchi, V. D.; Koster, L. J. A.; Blom, P. W. M.; Melzer, C.; de Boer, B.; van Duren, J. K. J.; Janssen, R. A. J. *Adv. Funct. Mater*. **2005**, *15*, 795−801.
(7) van Duren, J. K. J.; Yang, X. N.; Loos, J.; Bulle-Lieuwma, C. W. T.; Sieval, A. B.; Hummelen, J. C.; Janssen, R. A. J. *Adv. Funct. Mater*. **2004**, *14*, 425−434.
(8) Bassler, H. *Phys. Status Solidi B* **1993**, *175*, 15−56.
(9) Novikov, S. V.; Dunlap, D. H.; Kenkre, V. M.; Parris, P. E.; Vannikov, A. V. *Phys. Rev. Lett*. **1998**, *81*, 4472−4475.
(10) Parris, R. E.; Kenkre, V. M.; Dunlap, D. H. *Phys. Rev. Lett*. **2001**, *8712*, 126601.
(11) Chatten, A. J.; Tuladhar, S. M.; Nelson, J. *Proc. IEEE Photovoltaic Specialists Conference*, 31st, 2005; p 31−36.
(12) Tuladhar, S. M.; Choulis, S. A.; Chatten, A. J.; Bradley, D. D. C.; Nelson, J., to be submitted for publication.
(13) Sylvester-Hvid, K. O.; Rettrup, S.; Ratner, M. A. *J. Phys. Chem. B* **2004**, *108*, 4296−4307.
(14) Peumans, P.; Uchida, S.; Forrest, S. R. *Nature* **2003**, *425*, 158−162.
(15) Watkins, P. K.; Walker, A. B.; Verschoor, G. L. B. *Nano Lett*. **2005**, *5*, 1814−1818.
(16) Sariban, A.; Binder, K. *J. Chem. Phys*. **1987**, *86*, 5859−5873.
(17) Chatten, A. J.; Tuladhar, S. M.; Choulis, S. A.; Bradley, D. D. C.; Nelson, J. *J. Mater. Sci*. **2005**, *40*, 1393−1398.
(18) Bredas, J. L.; Calbert, J. P.; da Silva, D. A.; Cornil, J. *Proc. Natl. Acad. Sci. U.S.A*. **2002**, *99*, 5804−5809.
(19) Nelson, J. *Phys. Rev. B* **1999**, *59*, 15374−15380.
(20) Borsenberger, P. M.; Weiss, D. S. *Organic Photoreceptors for Xerography*; Marcel Dekker Inc.: New York, 1998.
(21) Although complete segregation can be achieved after many (over 10^{11}) moves in homophilic systems, we chose to stop the simulation when it reaches a quasi equilibrium after 10^9 because experimental studies of polymer-blend morphologies (ref 22) show that solvent evaporation typically leaves the materials "frozen" into a nonequilibrium morphology, rather than achieving complete segregation. We note here that our method could be used to simulate the effects of solvent on morphology (and also transport) using blend morphologies resulting from different numbers of snakes moves, that is, using lattices of different "maturity".
(22) Arias, A. C.; MacKenzie, J. D.; Stevenson, R.; Halls, J. J. M.; Inbasekaran, M.; Woo, E. P.; Richards, D.; Friend, R. H. *Macromolecules* **2001**, *34*, 6005−6013.
(23) Kreouzis, T.; Poplavskyy, D.; Tuladhar, S. M.; Campoy-Quiles, M.; Nelson, J.; Campbell, A. J.; Bradley, D. D. C. *Phys. Rev. B*, in press, 2006.
(24) Mozer, A. J.; Sariciftci, N. S. *Chem. Phys. Lett*. **2004**, *389*, 438−442.
(25) Persistence of Vision (TM) Raytracer. Persistence of Vision Pty. Ltd., Williamstown, Victoria, Australia. http://www.povray.org/
(26) Kline, R. J.; McGehee, M. D.; Kadnikova, E. N.; Liu, J. S.; Frechet, J. M. J. *Adv. Mater*. **2003**, *15*, 1519.
(27) Erb, T.; Zhokhavets, U.; Gobsch, G.; Raleva, S.; Stuhn, B.; Schilinsky, P.; Waldauf, C.; Brabec, C. J. *Adv. Funct. Mater*. **2005**, *15*, 1193−1196.
(28) Nelson, J. *Phys. Rev. B* **2003**, *67*, 155209.
(29) Offermans, T.; Meskers, S. C. J.; Janssen, R. A. J. *J. Chem. Phys*. **2003**, *119*, 10924−10929.
(30) Pivrikas, A.; Juska, G.; Mozer, A. J.; Scharber, M.; Arlauskas, K.; Sariciftci, N. S.; Stubb, H.; Osterbacka, R. *Phys. Rev. Lett*. **2005**, *94*, 176806.

NL0608386